ELSEVIER

Chemical Physics 235 (1998) 297–312

Chemical Physics

Numerical simulations of solvation in simple polar fluids: dependence on the thermodynamic state below and above the critical point

Peter Graf, Abraham Nitzan

School of Chemistry, Tel Aviv University, Tel Aviv 69978, Israel

Received 8 December 1997

Abstract

The dependence of solvation dynamics on the thermodynamic state of the solvent is studied numerically for simple model polar solvents. The solvent is described by the Stockmayer model, characterized by Lennard-Jones and dipolar intermolecular interactions. The solute–solvent coupling is given by a nonpolar (Lennard-Jones) and, for a charged solute, by a charge-dipole interaction. We study thermodynamic states which are representative of the liquid and vapor phases, of the neighborhood of the critical point, and of the supercritical region of the solvent. Statics and dynamics are studied by investigating equilibrium fluctuations in the electrostatic potential induced by the solvent at the solute position and the fluctuations in the nonpolar part of the solute–solvent interaction. The relaxation of these fluctuations corresponds, within linear response theory, to the dynamics of nonequilibrium solvation, and the applicability of linear response can be glimmed from comparing the results obtained for charged and uncharged solutes. For a few selected thermodynamic states, we also simulate the corresponding nonequilibrium solvation, starting from either a neutral or a charged solute. We find that both static and dynamical aspects of the solvation process are strongly affected by the density of the neat solvent. Effects of temperature are less pronounced. On lowering the solvent density, the relaxation of dynamic fluctuations gets increasingly more dependent on the solute charge, i.e. the validity of a linear response description decreases. The main characteristics of the dynamics can be largely traced to aspects of static structure. In addition, the effect of proximity to the critical point on the solvent static and dynamic response is examined.

1. Introduction

Recent work on solvation dynamics in polar liquids (e.g. [1–4] and references cited therein) has focused on the study of system response to a sudden change in the charge distribution of the solute. The typical quantity of interest in such studies is the solvation function

$$S(t) = \frac{\langle \Delta E(t)\rangle - \langle \Delta E(\infty)\rangle}{\langle \Delta E(0)\rangle - \langle \Delta E(\infty)\rangle}, \qquad (1)$$

where $\langle \Delta E(t)\rangle$ is an ensemble average of the change in the solute–solvent interaction energy observed at time t after a sudden change in the solute charge distribution at time $t = 0$. In the linear response regime the function $S(t)$ is well approximated by an equilibrium correlation function. For a sudden change in the magnitude of a solute point charge, this correlation function is given by

$$C_V(t) = \frac{\langle \delta V(t)\,\delta V(0)\rangle}{\langle \delta V^2\rangle}, \qquad (2)$$

where $\delta V(t) = V(t) - \langle V\rangle$ are the fluctuations in

0301-0104/98/$19.00
PII: S0301-0104(98)00058-5

the electrical potential $V(t)$ induced by the solvent at the solute position. Numerical simulations have shown that the linear response assumption works reasonably well for many cases of polar solvation [5–11], although cases where it does not hold have been reported [5,12–15].

Most experimental studies on polar solvation and consequently theoretical and numerical simulation work have focused on systems at ambient temperature and pressure. Recent studies have considered solvation in different regions of the thermodynamic phase space, mostly focusing on equilibrium aspects of solvation in supercritical nonpolar solvents [16–19]. In this paper we use numerical simulations to investigate issues of solvation in polar solvents under variation of the thermodynamic state of the solvent. In particular, we focus on the dependence of equilibrium and nonequilibrium solvation on variations of the solvent density and temperature. The thermodynamic states considered are representatives of the liquid and of the vapor phases, and of the critical and supercritical regions. Since we examine generic issues we have chosen a generic model for the solution: A spherical solute, either neutral or with a point charge at its center, in a Stockmayer fluid characterized by a combination of Lennard-Jones (LJ) and dipolar interaction. This model was used in the past to study classical solvation dynamics under ambient temperature and pressure [9–11], and these studies are extended here to other thermodynamic regimes: coexisting liquid and gas phases, the vicinity of the solvent critical point and the supercritical region. The latter thermodynamic regime is of interest both because of the importance of supercritical solvents in current technologies [20,21] and in view of recent experimental and numerical studies [22–26,16–19]. These studies indicate that the thermodynamic character of solvation in a supercritical solvent is very different from the corresponding process at ambient conditions for at least three reasons: (a) The dielectric constant of a supercritical solvent is considerably lower than that of the corresponding normal solvent and can be varied continuously by changing temperature and density; therefore dielectric saturation effects and ionic association may be more pronounced. (b) Solvent clustering about the solute molecule may be an important factor in the supercritical solvent response, especially in the low density regime. (c) Near the critical point solvent compressibility is large, and this may increase the relative importance of electrostriction (i.e. translational as opposed to rotational relaxation) in the solvation process. In particular, the possible importance of such effects in supercritical solvation suggests that the validity of linear response theory in the description of solvation thermodynamics and dynamics may strongly depend on the solvent density. These issues will be addressed by the present numerical experiments.

At the critical point some aspects of the solvent response become singular. While it is not clear that this singular character of the solvent will show itself in the relatively local phenomenon of solvation, it is interesting to examine several static and dynamic characteristics of the solvation process as we go through the critical region to see if some signature of critical behavior appears. We find, in agreement with earlier observations in other systems [22–24], that the transition through the critical region does show itself in some of the solvation properties, although in view of the limited number of thermodynamic states investigated and of the finite, relatively small size of the systems studied, the magnitude and significance of the effect should not be deduced from the results of the present simulations.

In the following section we describe the simulation procedure. Section 3 considers the equilibrium aspects of the solvation process, and the solvation structure. In Section 4, we present the results of our dynamical studies and discuss the dependence of the dynamical response on solvent density and temperature, as well as the validity of linear response. We summarize our findings in Section 5.

2. Simulation procedure

The Stockmayer solvent is characterized by its mass M, moment of inertia I, dipole moment μ, and the Lennard-Jones parameters ϵ and σ. The solute properties are determined by its charge q and mass M_s, and by the Lennard-Jones parameters for the solute–solvent interaction, ϵ_s and σ_s. The solute–solvent interaction is thus a superposition of short range Lennard-Jones potential and electrostatic charge-dipole interactions. Each of the simulated systems contains N particles in a cubic box of side

length L (volume $V = L^3$), subject to periodic boundary conditions. All pair interactions are cut off at a distance $R_c = L/2$. The electrostatic interactions are supplemented by terms associated with reaction field boundary conditions. Further details and expressions for the interaction potentials are given in Appendix A.

The solvent parameters are taken to approximate trifluoromethane (CHF_3), using a recent compilation of Stockmayer potential parameters determined from phase coexistence data [27]: $\mu = 1.62$ D, $\epsilon/k_B = 199.6$ K (k_B is the Boltzmann constant) and $\sigma = 4.007$ Å, and using $M = 70.01$ amu and $I = 48.52$ amu Å^2. We determined the latter (I) using the structure of CHF_3 in the liquid phase [28]. In reduced units ($\epsilon^* = 1$, $\sigma^* = 1$, $M^* = 1$) we get $\mu^* = \mu/(\epsilon\sigma^3)^{1/2} = 1.217$ and $I^* = I/(M\sigma^2) = 0.04316$. The unit of time is $(M\sigma^2/\epsilon)^{1/2} \approx 2.6$ ps. In these reduced units, values for the number density $\rho = N/V$ and the temperature T are determined by $\rho^* = \rho\sigma^3$ and $T^* = k_B T/\epsilon$. In the simulations described here the molecular parameters are held fixed while the thermodynamic state of the solute is varied. For simplicity we take $\epsilon_s = \epsilon$, $\sigma_s = \sigma$ and $M_s = M$. The solute charge is varied between $q = 0$ au and $q = 1$ au. In a typical simulation we use $N = 256$ particles.

For the implementation of the reaction field boundary conditions as well as for comparison with dielectric (continuum) theories of solvation, the value of the dielectric constant ϵ_0 of our neat solvent in the different thermodynamic states is needed. For a pure Stockmayer fluid, ϵ_0 was shown to satisfy well the following polynomial relation [29]:

$$\epsilon_0(y) = 1 + 2.932\,y + 4.210\,y^2 - 1.323\,y^3 + 0.6115\,y^4, \quad 0 \le y \le 3.31, \tag{3}$$

where the dipolar strength y is given in terms of the solvent number density $\rho = N/V$, the molecular dipole μ and the temperature T by

$$y = \frac{4\pi\rho\mu^2}{9k_B T}. \tag{4}$$

The ϵ_0 values determined by Eqs. (3) and (4) for our systems are then used for the exterior dielectric constant ϵ' which appears in the reaction field boundary conditions (see Appendix A) and for comparison with analytical models (in Sections 3 and 4). Taking the exterior dielectric constant ϵ' to be equal to the ϵ_0 value determined by Eqs. (3) and (4) rather than computing it self-consistently for each thermodynamic state is expected to be of minor influence on the data reported in the present work, since the precise value of ϵ' was shown to be of weak influence on the coexistence properties and the structure of coexisting phases [30], as well as on the simulated dynamics [9]. Note that we use the same ϵ_0 values for both the neat solvent and the corresponding solute–solvent system (where one solute particle has been replaced by the solute). This scheme conforms with the assumption of a dilute solution.

The thermodynamic states of the neat solvent are studied using the Gibbs ensemble Monte Carlo technique, originally introduced by Panagiotopoulos [31] and later applied by others to the investigation of vapor-liquid equilibria of Stockmayer fluids [32–34,27,30]. In the present simulations we follow the Monte Carlo sampling procedure of van Leeuwen et al. [33] while using reaction field boundary conditions as described by Garzón et al. [30]. We determined the values of the critical temperature T_c and of the critical density ρ_c following the common procedure [32–34,27,30] by fitting the numerical data to the scaling law $\rho_l - \rho_v = A \cdot (T_c - T)^\beta$ (where ρ_l and ρ_v are, respectively, the densities of the coexisting liquid and vapor determined by a simulation at temperature T, and where the value $\beta = 0.32$ was taken to be fixed during the fitting procedure) and to the law of rectilinear diameters, $(\rho_l + \rho_v)/2 = \rho_c + B \cdot (T_c - T)$. In using this procedure we have followed others in disregarding subtle issues associated with the approach to criticality in finite systems, such issues were investigated by Mon and Binder [35].

Following this procedure, we determined the approximate vapor–liquid coexistence curve of our neat solvent using a total of 512 particles in the two coexisting phases. The critical point of our Stockmayer ''CHF_3'' fluid is obtained in this way to be $(\rho_c^*, T_c^*) = (0.31, 1.50)$ in agreement with van Leeuwen [34,27] and the resulting coexistence diagram is shown in Fig. 1. Points on this diagram will be denoted by the corresponding values of the reduced density and temperature as (ρ^*, T^*). In Sec-

tion 4, we consider solvent dynamics and response in several thermodynamic states, marked on the phase diagram of Fig. 1 and denoted by (ρ_i^*, T_j^*), $i = 1,2,3$ and $j = 1,2,3$. The corresponding values of density and temperature are $\rho_1^* = 0.10$, $\rho_2^* = 0.31$, $\rho_3^* = 0.56$ and $T_1^* = 1.40$, $T_2^* = 1.50$, $T_3^* = 1.60$. Additional properties of these states are summarized in Table 1. Note that $\rho_2^* = \rho_c^*$ and $T_2^* = T_c^*$. (ρ_1^*, T_1^*) and (ρ_3^*, T_1^*) correspond to the boundaries of the vapor-liquid coexistence region at T_1^*. The states with $T^* = T_2^*$ display density change at the critical temperature, while the states with $T^* = T_3^*$ correspond to the supercritical regime.

Once the equilibrium thermodynamic states of interest were determined, ensembles of corresponding equilibrium configurations were generated for these states using (regular NVT) Monte Carlo (MC) evolution with Metropolis sampling. Typically, each tenth MC-cycle is sampled during this production of equilibrium data. Reported data for static fluctuations and structure (Section 3) is extracted from 5000 such configurations for each thermodynamic state investigated. Dynamics of the system (Section 4) was studied by classical molecular dynamics (MD) simulations using the velocity Verlet algorithm with a time step of $\Delta t \approx 1.033$ fs. These MD runs are

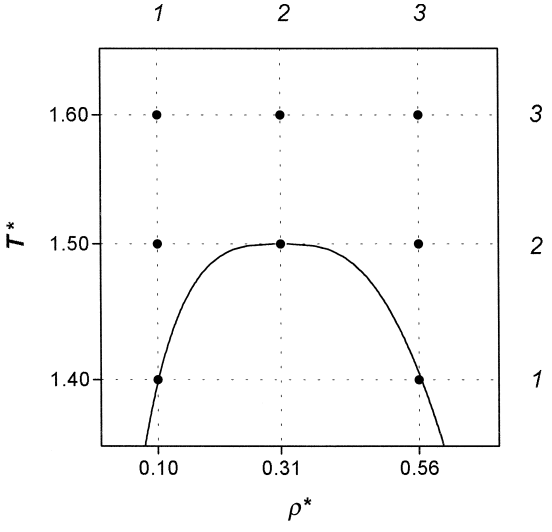

Fig. 1. The vapor-liquid coexistence curve of the simulated model CHF_3 solvent. The eight dots indicate the thermodynamic states investigated in this work. These states are denoted in the text by (ρ_i^*, T_j^*) with $i = 1,2,3$ and $j = 1,2,3$ and the corresponding values of ρ_i^* and T_j^* are noted in the figure.

Table 1
The dipolar strength y and the corresponding dielectric constant $\epsilon_0(y)$ from the polynomial relation for the dielectric constant (Eqs. (3) and (4)) for the different thermodynamic states indicated in Fig. 1

		ρ_1^*	ρ_2^*	ρ_3^*
T_3^*	y	0.13	0.40	0.72
	$\epsilon_0(y)$	1.45	2.78	4.99
T_2^*	y	0.14	0.43	0.77
	$\epsilon_0(y)$	1.48	2.94	5.38
T_1^*	y	0.15		0.83
	$\epsilon_0(y)$	1.52		5.84

similar to those described by Neria et al. [9], except that the absolute magnitude of the molecular dipole was kept fixed using the RATTLE (instead of the SHAKE) algorithm [36]. The system was brought to the desired temperature using Andersen thermalization [37]. Reported data for the dynamics of equilibrium fluctuations is extracted from trajectories of a total length of ≈ 500 ps. Data for nonequilibrium solvation are averages over 50 runs, each starting from an initial configurations taken from the equilibrium MD simulations (at 100 fs intervals). All MC and MD simulations were done at constant number of particles and volume.

3. Equilibrium aspects

Some observations concerning the equilibrium structure associated with solvation in the different thermodynamic states of our model solvent are discussed in this section. We focus on the average electrostatic potential $\langle V \rangle$ at the solute position (the reaction potential), on the average nonpolar (LJ) part of the solute–solvent interaction, $\langle U_{LJ} \rangle$, on the corresponding fluctuation amplitudes $\langle \delta V^2 \rangle$ and $\langle \delta U_{LJ}^2 \rangle$ and on structural aspects expressed by the distribution functions for the solvent density and for the polarization density about the solute. These distribution functions are, respectively,

$$g_0(r) = \frac{1}{\rho}\left\langle \sum_{i=1}^{N} \delta(\boldsymbol{r} - \boldsymbol{R}_{si}) \right\rangle \tag{5}$$

and

$$g_1(r) = \frac{1}{\rho}\left\langle \sum_{i=1}^{N} \frac{\boldsymbol{\mu}\cdot\boldsymbol{R}_{si}}{\mu R_{si}} \delta(\boldsymbol{r} - \boldsymbol{R}_{si}) \right\rangle, \tag{6}$$

where $\boldsymbol{R}_{si} = \boldsymbol{R}_s - \boldsymbol{R}_i$ with the solute position $\boldsymbol{R}_s$ and the solvent particle positions $\boldsymbol{R}_i$. In addition, it is of interest to consider the number of solvent particles $\overline{N}(r_0)$ within a neighborhood of radius r_0 about the solute. If r_0 is the radius of the first solvation shell, $\overline{N}(r_0)$ measures the ''coordination number'' about the solute. The normalized difference,

$$\bar{n}(r_0;q) = \left[\overline{N}(r_0;q) - \overline{N}(r_0;q=0)\right]\Big/\overline{N}(r_0;q=0), \quad (7)$$

where q is the solute charge, is a measure of the electrostriction effect. In the computations reported below we have used $r_0 = 1.5\sigma$ which lies (see Fig. 2) between the first and second peaks of the pair correlation function for the ''normal fluid'', i.e. the fluid in the liquid state (ρ_3^*, T_1^*). In addition, we consider the average distance $\overline{r}_s$ and the average orientation $\overline{\cos\theta}_s$ relative to the solute–solvent axis of the N_s solvent molecules nearest to the solute. We have chosen $N_s = 8$, which was found to be the order of the coordination number in the state (ρ_3^*, T_1^*) (Fig. 4).

In what follows we focus on the solvent states $(\rho_1^*, T_1^*) = (0.10, 1.40)$, $(\rho_3^*, T_1^*) = (0.60, 1.40)$, $(\rho_2^*, T_2^*) = (0.31, 1.50)$ and $(\rho_2^*, T_3^*) = (0.31, 1.60)$ (see Fig. 1). The first two are vapor and liquid phases at coexistence, while the latter two are in the critical and supercritical region, respec-

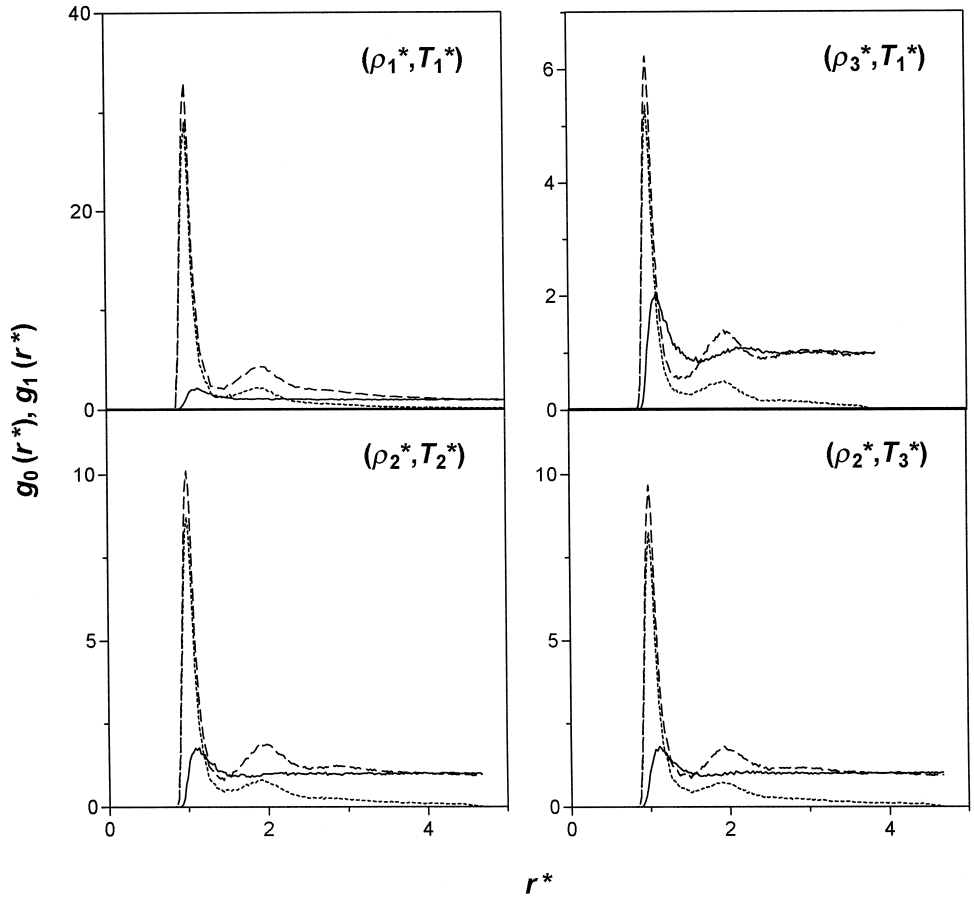

Fig. 2. Distribution functions of the solvent around the solute. Shown are results for the four thermodynamics states (ρ_1^*, T_1^*), (ρ_3^*, T_1^*), (ρ_2^*, T_2^*), and (ρ_2^*, T_3^*). The full and dashed lines show the solvent density (g_0, Eq. (5)) at a distance r from a neutral ($q = 0$) and charged ($q = 1$) solute respectively. The dotted lines show the (negative) polarization density ($-g_1$, Eq. (6)) for solute charge $q = 1$. Note that the ranges displayed for the distribution functions g are different for the different subfigures.

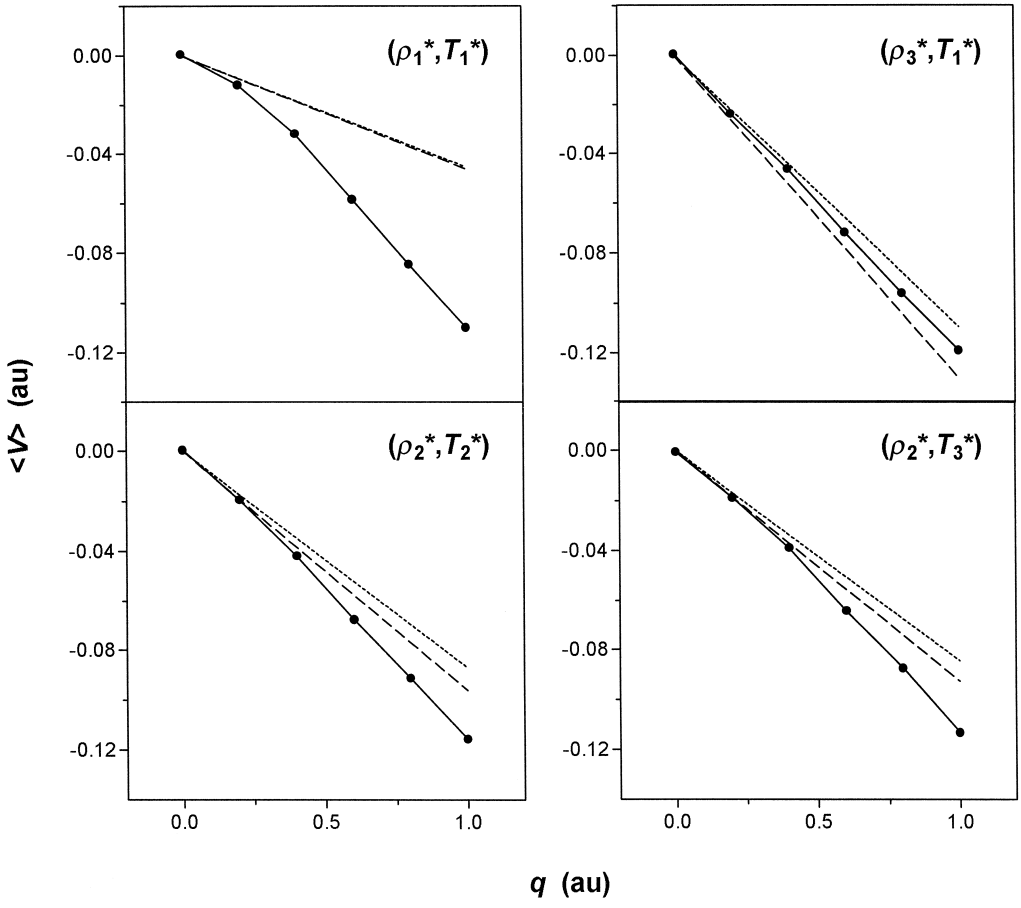

Fig. 3. The reaction potential $\langle V \rangle$ versus solute charge q for the same four thermodynamic states as in Fig. 2. The full lines connect the results from Monte Carlo simulations. The dotted and dashed lines correspond to the Born and the MSA models (Eqs. (9) and (10)–(11)), respectively.

tively. Fig. 2 shows the distribution functions $g_0(r)$ and $g_1(r)$ in these states for solutes with point charge $q = 0$ or $q = 1$. Fig. 3 shows the dependence of the reaction potential $\langle V \rangle$ on the solute charge q. The reaction potential is related to the solvation free energy W_{solv} by

$$W_{\text{solv}} = \int_0^q \langle V \rangle \, \mathrm{d}q' . \tag{8}$$

Under linear response, where $\langle V \rangle$ depends linearly on the solute charge q', this yields $W_{\text{solv}} = q\langle V \rangle/2$. Fig. 3 shows that in the range $q = 0 \ldots 1$ $\langle V \rangle$ depends approximately linearly on q in all but the vapor system (ρ_1^*, T_1^*). In the latter and to some extent in the critical and supercritical system a significant super-linearity arises from the highly compressible nature of the solvent which strongly promotes electrostriction. Note that saturation of dipolar orientation is another potential source of nonlinearity. In fact, electrostriction and dielectric saturation appear to affect the evolution of the reaction potential in an opposite manner, because the latter by itself is expected to lead to a sublinear evolution with increasing solute charge (see also Refs. [38,7]). The superlinear behavior seen in Fig. 3 indicates that electrostriction is the dominant source of nonlinear response in this regime. Also shown in Fig. 3 are theoretical results for $\langle V \rangle$, given by the Born ex-

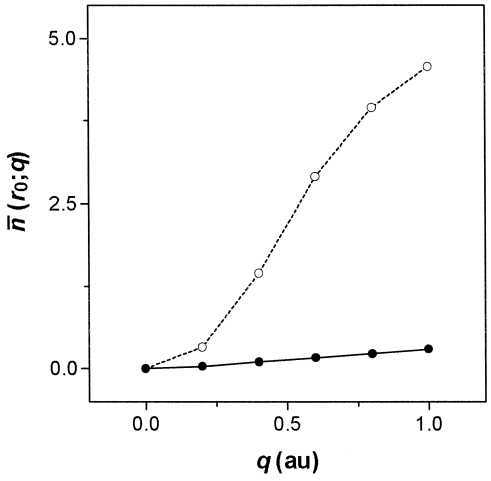

Fig. 4. Normalized difference in number of solvent particles (Eq. (7)) in a sphere of radius $r_0 = 1.5\sigma$ centered about the solute. The full line connects the simulation results for the liquid state (ρ_3^*, T_1^*); the dotted line is the corresponding result for the vapor state (ρ_1^*, T_1^*).

pression using for the cavity radius the LJ diameter σ,

$$\langle V\rangle_{\mathrm{Born}} = -\frac{q}{\sigma}\left(1-\frac{1}{\epsilon_0}\right), \tag{9}$$

where the values for ϵ_0 were taken as the corresponding $\epsilon_0(y)$ values from Table 1, and by the mean spherical approximation (MSA) [39–41],

$$\langle V\rangle_{\mathrm{MSA}} = -\frac{q}{R}\left(1-\frac{1}{\epsilon_0}\right)(1+\Delta)^{-1}, \tag{10}$$

$$\Delta \cong \frac{3r_{\mathrm{solv}}}{R}\left(108^{1/3}\epsilon_0^{1/6}-2\right)^{-1}, \tag{11}$$

where R and r_{solv} (both equal here to $\sigma/2$) are respectively the solute and solvent radii. We see that these theoretical linear response expressions account relatively well for the behavior of the normal liquid state and perform more poorly for the more compressible vapor, critical and supercritical states. For the vapor phase, where solvation is primarily associated with the formation of a solvent droplet around the charged solute, the linear response expressions with the vapor dielectric response fail badly.

The most important qualitative difference between solvation in relatively incompressible fluid states such as (ρ_3^*, T_1^*) and between the corresponding behavior of a compressible fluid, e.g. the coexisting vapor at (ρ_1^*, T_1^*), is the solvation structure in the neighborhood of the solute molecule. This is shown in Fig. 4 which depicts the normalized difference $\bar{n}(r_0;q)$ (Eq. (7), for $r_0 = 1.5\sigma$) for the coexisting liquid and vapor phases and in Fig. 5 where $\bar{r}_{\mathrm{s}}$ and $\overline{\cos\theta}_{\mathrm{s}}$ (for $N_{\mathrm{s}} = 8$) are displayed as functions of solute charge q for the same coexisting fluids. Also shown in Fig. 5 are the electrostatic potential $\langle V\rangle_{\mathrm{s}}$ and the Lennard-Jones energy $\langle U_{\mathrm{LJ}}\rangle_{\mathrm{s}}$ induced by the solvent at the solute position, taken as an average over the $N_{\mathrm{s}} = 8$ solvent molecules nearest to the solute. The evolution of these quantities with increasing q clearly shows that in the vapor phase, a liquid-like neighborhood is developed near the solute with increasing q. For $q = 1$ the properties of the first solvation shell in the coexisting liquid and vapor of our solvent are quite similar. This is also seen in the results (Table 2) for the average electrostatic and Lennard-Jones potential, $\langle V\rangle$ and $\langle U_{\mathrm{LJ}}\rangle$ respectively, induced by the solvent at the solute position, and for the corresponding fluctuation amplitudes $\langle \delta V^2\rangle$ and $\langle \delta U_{\mathrm{LJ}}^2\rangle$. The theoretical results in Table 2 were calculated by Eqs. (9)–(11) and by the corresponding expressions

$$\langle \delta V^2\rangle_{\mathrm{Born}} = \frac{k_{\mathrm{B}}T}{a}\left(1-\frac{1}{\epsilon_0}\right) \tag{12}$$

and

$$\langle \delta V^2\rangle_{\mathrm{MSA}} = \frac{k_{\mathrm{B}}T}{R}\left(1-\frac{1}{\epsilon_0}\right)(1+\Delta)^{-1}. \tag{13}$$

It is seen that for the charged solute these properties are quite similar in the coexisting vapor (ρ_1^*, T_1^*) and liquid (ρ_3^*, T_1^*) phases. This similarity is associated with the fact (exaggerated by the finite size of our simulation cell) that these properties are dominated by the close neighborhood of the solute molecule. However, the development of the solvation structure in the two solvents is quite different, and is consistent with the marked nonlinear response associated with the more compressible liquid. We also note that the results for the *equal density* critical and supercritical states, (ρ_2^*, T_2^*) and (ρ_2^*, T_3^*), are very similar.

The observation just made may reasonably suggest that the proximity of the critical point does not

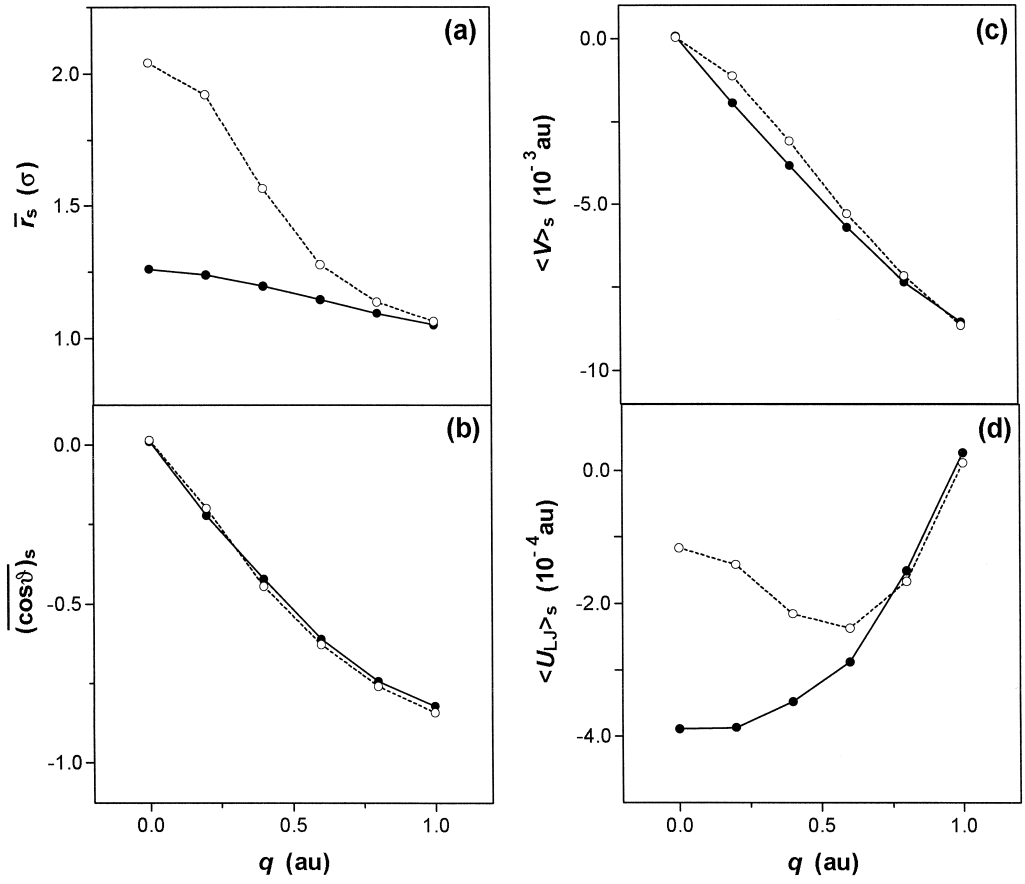

Fig. 5. Properties of the local solvation neighborhood as function of solute charge: (a) Average distance $\bar{r}_s$ of the $N_s = 8$ solvent molecules closest to the solute; (b) average orientation $\overline{\cos\theta}_s$ relative to the solute–solvent axis of the same N_s solvent molecules; (c) and (d) similar averages for the electrostatic ($\langle V\rangle_s$) and nonpolar ($\langle U_{LJ}\rangle_s$) parts of the solute–solvent interaction respectively. All results are shown versus solute charge q. Line notation is as in Fig. 4.

have a special effect on the solvation which is an essentially local phenomenon. Fig. 6, however, indicates that some effect may be expected. Here the solvent density in the first solvation shell, ρ_1, defined by $0.5 < r^* < 1.5$ ($r = r/\sigma$ is the dimensionless distance from the solute center), and the second solvation shell, ρ_2, $1.5 < r^* < 2.5$, are plotted for the charged solute against the bulk solvent density ρ at the critical temperature. Because of electrostriction ρ_1 and ρ_2 are larger than ρ, however as ρ increases this difference is expected to diminish. It appears that the critical point, $\rho = \rho_c$, marks the transition above which ρ_1 and ρ_2 more rapidly approach ρ. Because of the small size of the simulated system this observation should be regarded as preliminary.

The different structural aspects of the solvation process should show up in the dynamics. While in the normal, less compressible fluid the dynamics may be dominated by solvent librations and rotations, in the compressible fluid electrostriction dynamics is expected to be more important. We turn into these dynamical aspects in the following section.

4. Dynamical aspects

We first consider the dynamics of equilibrium fluctuations, represented by the correlation function $C_V(t)$ (Eq. (2)) for solute charges $q = 0$ and $q = 1$.

Table 2
Average electrostatic and LJ potentials $\langle V\rangle$ and $\langle U_{LJ}\rangle$, and the corresponding fluctuation amplitudes $\langle \delta V^2\rangle^{1/2}$ and $\langle \delta U_{LJ}^2\rangle^{1/2}$, induced by the solvent at the solute center. Also shown, when applicable, are the Born and MSA results (Eqs. (9)–(13))

		(ρ_1^*, T_1^*)	(ρ_3^*, T_1^*)	(ρ_2^*, T_2^*)	(ρ_2^*, T_3^*)
$\langle V\rangle$	$q=1$	−0.11	−0.12	−0.12	−0.11
	Born	−0.045	−0.11	−0.087	−0.085
	MSA	−0.046	−0.13	−0.096	−0.093
$\langle \delta V^2\rangle^{1/2}$	$q=0$	0.0066	0.0094	0.0086	0.0087
	$q=1$	0.010	0.0098	0.0097	0.010
	Born	0.0063	0.0098	0.0091	0.0092
	MSA	0.0064	0.0107	0.0096	0.0096
$\langle U_{LJ}\rangle$	$q=0$	−0.00099	−0.0047	−0.0025	−0.0026
	$q=1$	−0.0013	−0.0022	−0.0017	−0.0017
$\langle \delta U_{LJ}^2\rangle^{1/2}$	$q=0$	0.00067	0.00096	0.00095	0.00098
	$q=1$	0.0023	0.0024	0.0025	0.0025

We will also consider the equivalent correlation function $C_{LJ}(t)$ for the LJ potential,

$$C_{LJ}(t) = \frac{\langle \delta U_{LJ}(t)\,\delta U_{LJ}(0)\rangle}{\langle \delta U_{LJ}^2\rangle}, \tag{14}$$

which is determined by the same solvent motions, but reflected through the short LJ interaction. Our results are summarized in Figs. 7 and 8, and Tables 3 and 4.

The short time dependence of equilibrium correlation functions of the type displayed in Figs. 7 and 8 should be rigorously given by $C(t) \sim 1 - \alpha t^2$, however it is convenient to fit the numerical results to a sum of a Gaussian and exponential decay,

$$C(t) = a\exp\left(-\frac{t^2}{2\tau_G}\right) + (1-a)\exp\left(-\frac{t}{\tau_E}\right). \tag{15}$$

Obviously such a fit does not capture the oscillations observed in many of the correlation functions displayed, but it provides a simple way of estimating the timescales of Gaussian and exponential relaxation processes. Tables 3 and 4 give the resulting fit parameters a, τ_G and τ_E for the correlation functions $C_V(t)$ and $C_{LJ}(t)$, respectively. Note that in some cases the exponential component of the relaxation cannot be observed within our numerical accuracy. For these cases the amplitude a was set to unity and the fit was done just for the Gaussian component. It is also interesting to note that in the case of $C_V(t)$ (Table 3) the Gaussian time τ_G for the *neutral* solute is in reasonably close agreement with the linear response theoretical values suggested by Maroncelli et al. [42],

$$\tau_G = \left[\frac{3I}{8\pi\rho\mu^2}\left(1 - \frac{1}{\epsilon_0}\right)\right]^{1/2}. \tag{16}$$

Results based on this expression are given in Table 3. However, as seen in Table 3, the relaxation times depend on the charging state of the solute, in contrast to the prediction of Eq. (16).

The following observations regarding the results displayed in Figs. 7 and 8 and in Tables 3 and 4 can be made:

(a) The solvent response, as expressed by the correlation functions $C_V(t)$ and $C_{LJ}(t)$, is often characterized by two main relaxation modes: A short time Gaussian-like behavior following by a long time exponential relaxation. The overall appearance of the relaxation process can be broadly characterized by the timescales of these components, by their relative amplitudes and by the period of the accompanying oscillations.

(b) The relaxation processes associated with the solvent response functions $C_V(t)$ and $C_{LJ}(t)$ depend

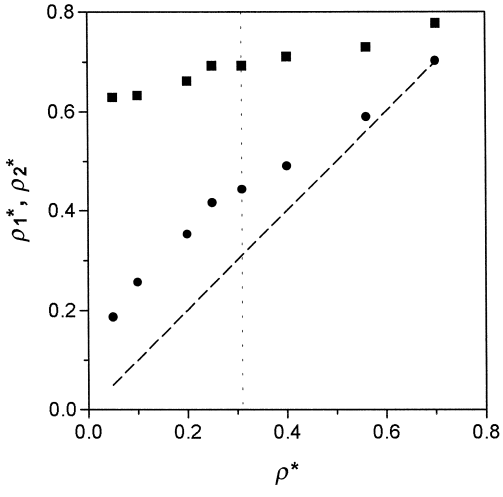

Fig. 6. Solvent density ρ_1^* (full squares) and ρ_2^* (full circles) in the first and second solvation shells, respectively, about a charged solute ($q=1$), plotted against the bulk solvent density at the critical temperature. The dotted vertical line marks the critical density.

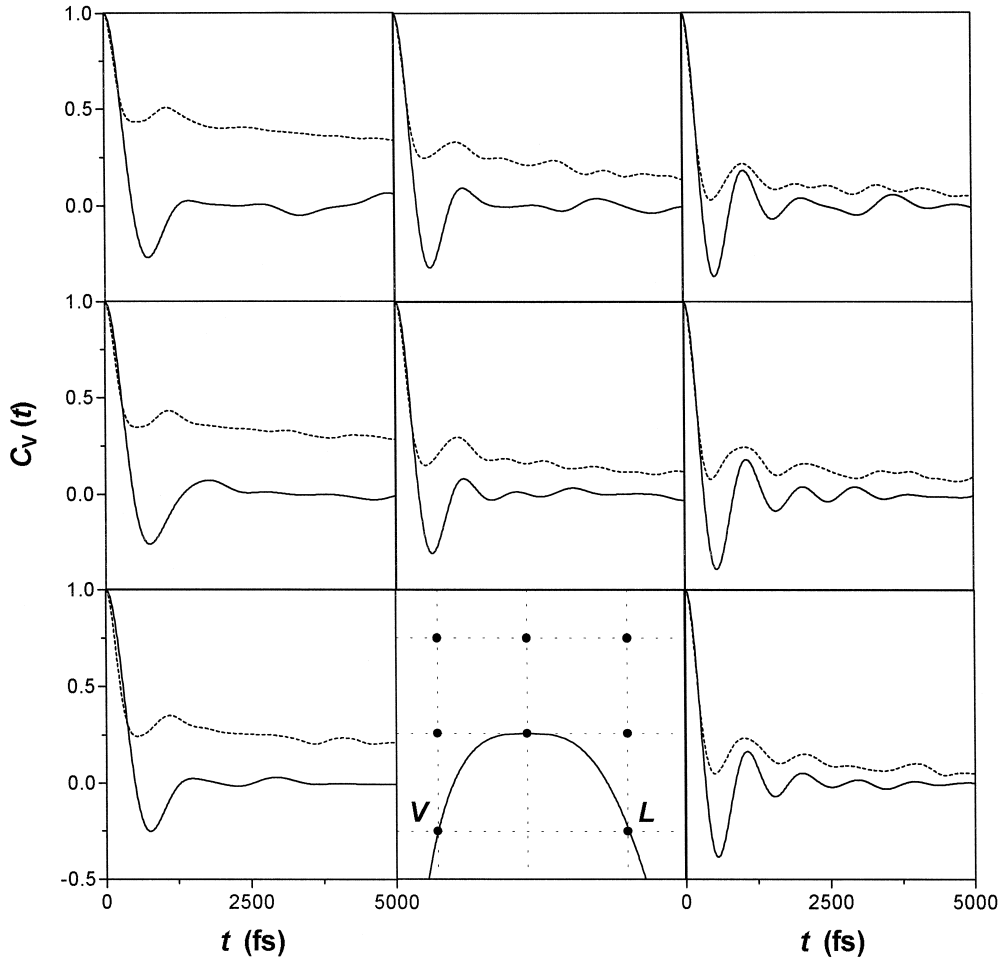

Fig. 7. Equilibrium correlation functions $C_V(t)$ (Eq. (2)) of the electrostatic potential induced by the solvent at the solute position. Note that the subfigures are positioned according to their position on the phase diagram (Fig. 1), shown also in the bottom center panel. Full and dotted lines correspond to solute charge $q = 0$ and $q = 1$, respectively.

strongly on the thermodynamic state of the solvent. Within the limited thermodynamic space that we explored we find that the character of the solvent response is mostly affected by its density.

(c) Comparing the behavior of the solvent relaxation about a charged $(q = 1)$ and an uncharged $(q = 0)$ solute, close to linear behavior (independence of solute charge) is seen for $C_V(t)$ at high T^* and ρ^*. Markedly different relaxation patterns for the two solute charges, indicating nonlinear response, appear in the gas phase and at the low density supercritical states. The dynamics of $C_{LJ}(t)$ shows a considerably stronger nonlinear behavior, which, again, is more pronounced for the lower density states. The dependence on temperature at constant density is much less pronounced.

(d) For $C_V(t)$ the amplitude of the long time relaxation process is larger about a charged solute then near a neutral solute (in the latter case the long time relaxation component cannot be observed within our numerical accuracy). Moreover, this amplitude is larger for the lower density fluid. For $C_{LJ}(t)$ this behavior is reversed: The long time component of the relaxation is not observed within our accuracy in the $q = 1$ case and it is very prominent in the $q = 0$ case — more so for the lower density fluid.

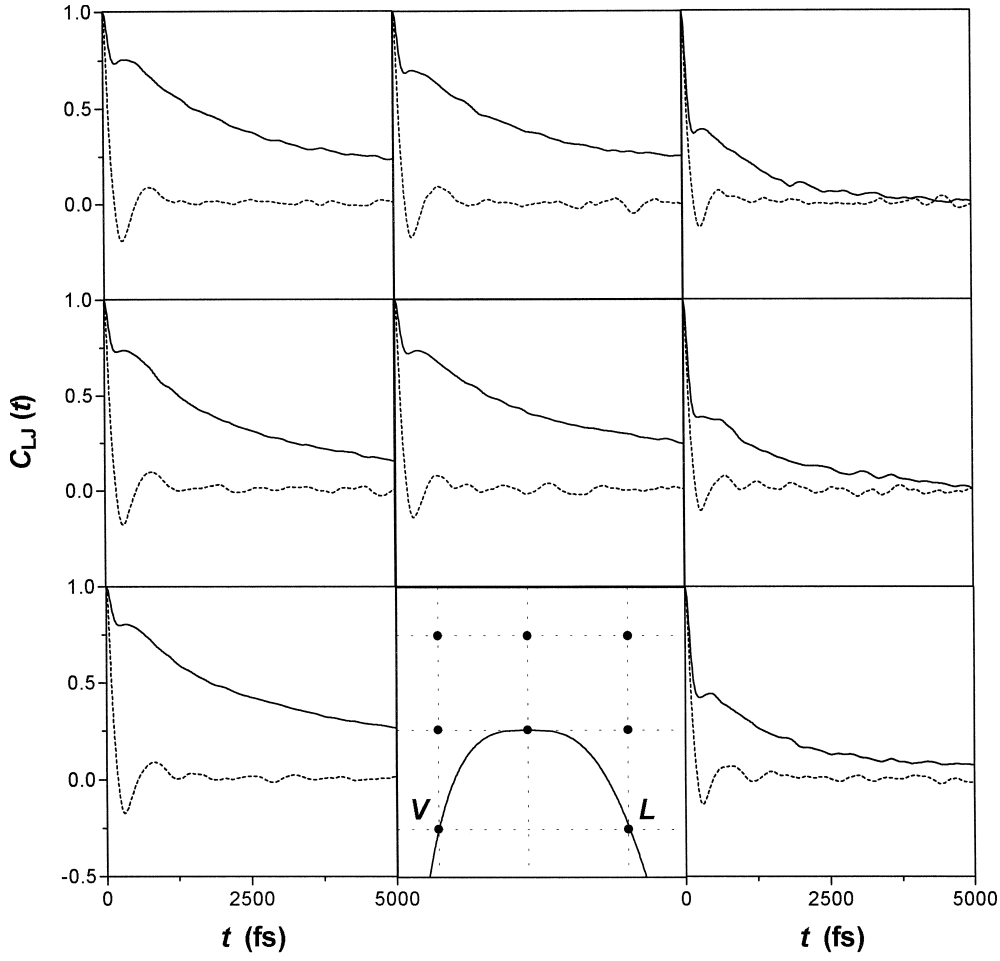

Fig. 8. Equilibrium correlation functions $C_{LJ}(t)$ (Eq. (14)) of the nonpolar part of the solute–solvent interaction. The layout and the line notation are the same as in Fig. 7.

The relaxation processes that affect $C_V(t)$ and $C_{LJ}(t)$ result from translational and rotational motions of solvent molecules. $C_{LJ}(t)$ is affected only by translational motions of solvent molecules close to the solute, while $C_V(t)$ is affected by both solvent translations and rotations, and contains contributions from solvent molecules farther from the solute. The qualitative behavior of the correlation functions shown in Figs. 7 and 8 can be explained by assuming that the bimodal character of the relaxation is associated with the approximate separability of molecular motions to those which occur within local potential wells and those which take place by crossing local potential barriers. When the first type dominates the relaxation, the corresponding correlation function is essentially described by the fast relaxation component with accompanying oscillations. When the second type becomes important, a slow component appears in the time evolution of the corresponding relaxation process.

It should be emphasized that the picture just outlined complements, not contradicts, the usual picture of solvation dynamics which associates the fast component with ''inertial response'' and the slow one with ''diffusive response'' (see, e.g., Refs. [7,9] and references cited therein). Inertial response, i.e. solvent response on a time scale not affected by the time dependence of intermolecular interactions, often

Table 3
Results of fits (Eq. (15)) to the normalized correlation function $C_V(t)$ (Fig. 7). The numbers in brackets are the theoretical predictions of Eq. (16). τ_G and τ_E are given in femtoseconds. Note that for the neutral solute the amplitude a was preset to unity and the fit was done only for the Gaussian component

		ρ_1^*		ρ_2^*		ρ_3^*	
		$q=0$	$q=1$	$q=0$	$q=1$	$q=0$	$q=1$
T_3^*	a	1	0.51	1	0.67	1	0.86
	τ_G	250 (269)	144	206 (220)	152	178 (183)	148
	τ_E		12930		6065		6624
T_2^*	a	1	0.60	1	0.75	1	0.80
	τ_G	250 (276)	149	211 (224)	148	180 (185)	143
	τ_E		14200		4412		5914
T_1^*	a	1	0.68			1	0.82
	τ_G	256 (284)	150			180 (187)	147
	τ_E		11380				4697

dominates — in particular in small molecules solvents — the short time relaxation. However, the inertial response is not a condition for the existence of the fast component [43]; the latter can be found also in models for solvation based on hopping motions, i.e. intrinsically without inertial response [44].

Consider now the relaxation behaviors displayed in Figs. 7 and 8. $C_V(t)$ (Fig. 7) is mostly affected by solvent rotations. For the neutral solute the solvent is not locally ordered and barriers to rotation are low. Most of the relaxation process takes place within local potential wells or through low (relative to k_BT) barriers. For $q=1$ the solvent is orientationally ordered in the vicinity of the charged solute. This implies relatively larger barriers to solvent rotations and a more prominent slow component in the relaxation. On the other hand, the time evolution of $C_{LJ}(t)$ (Fig. 8) is due to solvent translations within the nearest neighborhood (due to the short range of the LJ interaction) of the solvent. For $q=1$ this neighborhood is almost fixed since the solvent dipoles are strongly attracted to the solute, i.e. its relaxation consists of small amplitude arrangements within local potential wells. Therefore for $q=1$ all relevant relaxation is fast. Exchange of molecules in this neighborhood is possible only for the neutral solute, hence the existence of a prominent long time component in the relaxation for this case. In agreement with this, note the independence of the evolution of $C_{LJ}(t)$ on the solvent density observed for the charged solute case. The nearest neighborhood to the solute, i.e. the first solvation shell, does not depend on the bulk solvent density, in fact it can be thought of as a small droplet of solvent about the solute. Therefore the dynamics within this droplet is only weakly dependent on the bulk solvent density.

Next consider the relation between the linearity of the solvation process and the solvent density. The dependence of the solvent dielectric response on its density, together with the expectation and observation that the smaller the solvent density the larger is the dependence of the local environment of the solute on its charging state, imply that the nonlinear nature of the response will be more pronounced for the lower density solvent states. This is indeed observed in all the cases examined. We may conclude that the degree of nonlinearity in solvation should depend on the solvent compressibility, and more directly on the extent to which the density in the local neighborhood of the solute changes during the charging process.

Turning now to the nonequilibrium solvation functions $S(t)$ (Eq. (1)), we note that even though this function is defined in terms of the total solvation energy, i.e. electrostatic plus LJ interactions, the former dominates it quantitatively, and therefore the behavior of $S(t)$ (Fig. 9 and Table 5) is closely associated with that of the correlation function $C_V(t)$ (Fig. 7). The marked differences between the relaxation following the changes $q=0\rightarrow q=1$ and $q=1\rightarrow q=0$ is again an indication of the nonlinearity

Table 4
Results of fits (Eq. (15)) to the normalized correlation function $C_{LJ}(t)$ (Fig. 8). The times τ_G and τ_E are given in femtoseconds. Note that for the charged solute the amplitude a was preset to unity and the fit was done only for the Gaussian component

		ρ_1^*		ρ_2^*		ρ_3^*	
		$q=0$	$q=1$	$q=0$	$q=1$	$q=0$	$q=1$
T_3^*	a	0.19	1	0.27	1	0.50	1
	τ_G	55	69	62	71	58	72
	τ_E	3524		3919		1315	
T_2^*	a	0.18	1	0.22	1	0.52	1
	τ_G	53	72	62	71	63	73
	τ_E	2777		3525		1715	
T_1^*	a	0.15	1			0.49	1
	τ_G	70	73			65	75
	τ_E	3995				2074	

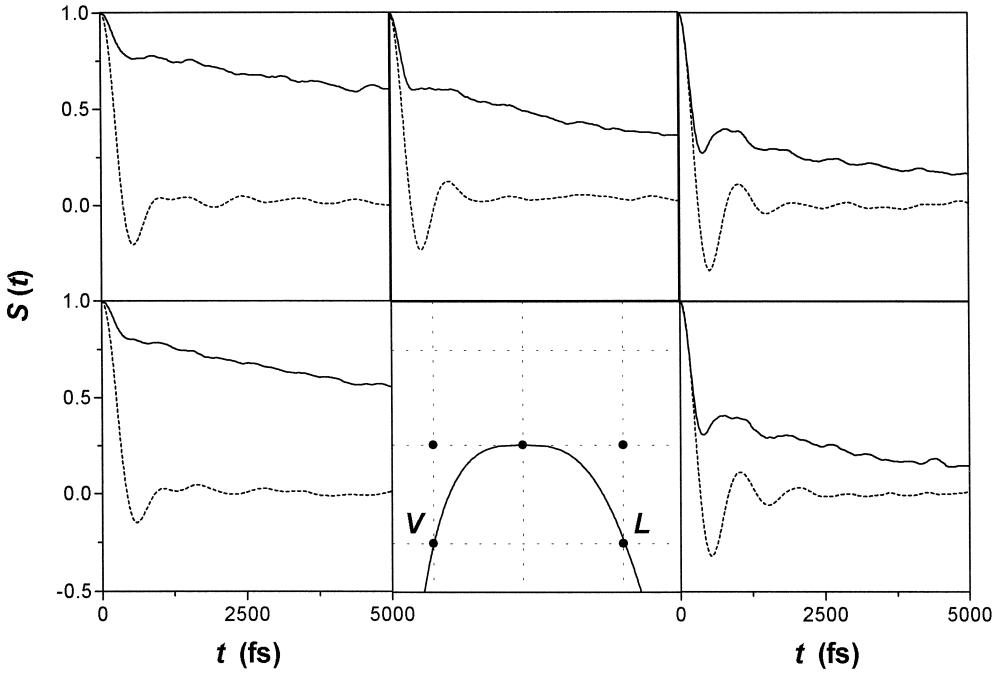

Fig. 9. The nonequilibrium solvation functions, $S(t)$ (Eq. (1)) of the total solute–solvent interaction energy for the solvent states with $T^* = T_1^*$ and T_2^* (coexisting vapor and liquid, and the critical temperature, respectively). Full and dotted lines correspond to the relaxations which follow the sudden $q = 0 \rightarrow q = 1$ and $q = 1 \rightarrow q = 0$ switches, respectively.

of the process. This difference is larger for the lower density solvent states, which is compatible with the observation that the lower density (and more compressible) solvents are less linear. Also note that the evolution following the $q = 1 \rightarrow q = 0$ switch is essentially complete on the short time scale, while that associated with $q = 0 \rightarrow q = 1$ process has a considerable long time component, in agreement with the argument made above that in the field of a charged solute solvent rotations have to overcome potential barriers which are absent in the case of a neutral solute. This characteristic is compounded by the fact that following a $q = 0 \rightarrow q = 1$ switch the solvent is compressing itself into the small solvation neighborhood of the solute, a slower process than the opposite expansion which takes place after the central charge changes from 1 to 0.

Finally consider the behavior of the solvent dynamical response near the critical point. Fig. 10 shows the exponential relaxation time τ_E plotted

Table 5
Results of fits (Eq. (15)) to the solvation function $S(t)$ (Fig. 9). The times τ_G and τ_E are given in femtoseconds. ρ_i^* $(i = 1,2,3)$ and T_j^* $(j = 1,2)$ are the density and temperature values indicated in Fig. 1

		ρ_1^*		ρ_2^*		ρ_3^*	
		$q = 0 \rightarrow 1$	$q = 1 \rightarrow 0$	$q = 0 \rightarrow 1$	$q = 1 \rightarrow 0$	$q = 0 \rightarrow 1$	$q = 1 \rightarrow 0$
T_2^*	a	0.19	1	0.34	1	0.60	1
	τ_G	171	206	141	190	129	174
	τ_E	15890		7816		5450	
T_1^*	a	0.16	1			0.61	1
	τ_G	172	219			139	183
	τ_E	11860				3082	

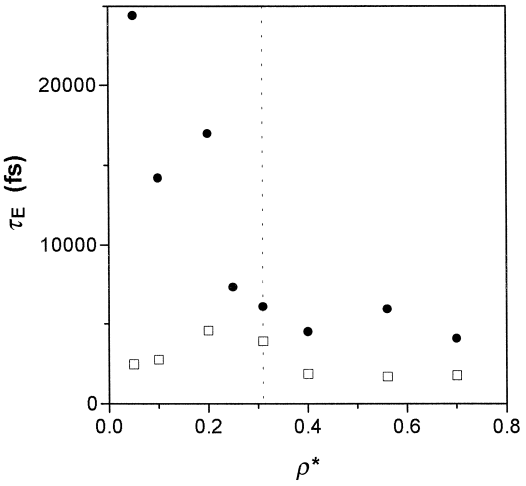

Fig. 10. The exponential relaxation time τ_E associated with the correlation function $C_V(t)$ for $q=1$ (full circles) and $C_{LJ}(t)$ for $q=0$ (blank squares) plotted against the bulk solvent density at the critical temperature. The dotted vertical line marks the critical density.

against the solvent bulk density at the critical temperature. As noticed above, a detectable exponential relaxation component is observed in $C_V(t)$ for $q=1$ and in $C_{LJ}(t)$ for $q=0$. The former shows a marked change of behavior at the critical density, from a rapidly diminishing trend for increasing ρ to essential independence of ρ above ρ_c. τ_G which has been shown [7] to depend mostly on the immediate vicinity of the solute does not show a similar trend. As noted before, in view of the small size of the simulated system and our limited statistics, these results should be considered preliminary.

5. Summary and conclusions

Using a Stockmayer model for a polar solvent and a spherical charged solute we have investigated the dependence of several equilibrium and dynamic characteristics of the solvation process on the thermodynamic state of the solvent. We found that for given solvent molecular properties, these characteristics depend mostly on the solvent density. In particular we found that the lower is the solvent density the stronger is the nonlinear character of the solvation response. This observation is related to the (intuitively obvious) fact that for a lower bulk solvent density, its equilibrium local density in the neighborhood of the solute is more sensitive to the solute charge. In fact it was seen that for a solute charge $q=1$ the local density in the first solvation shell for a liquid solvent is quite similar to that in the coexisting vapor. Dynamical implications of this behavior were observed and discussed.

We have found that the proximity of the critical point can show itself when some equilibrium and dynamical characteristics of the solvation are observed as functions of density near the critical temperature. We leave for future studies the question whether these observation are associated with real critical behavior of the solvation process.

Acknowledgements

This research was supported in part by the Israel Science Foundation and by the Kurt Lion Fund. P.G. is thankful to the Minerva-Stiftung for a postdoctoral fellowship.

Appendix A. Interaction potentials

The interaction potentials and boundary conditions used in this work are standard. Interaction energies are given as a sum of pairwise additive pair potentials. All pair interactions are cut off at a distance $R_c = L/2$, half the cubic box side length L.

The nonpolar part of the solvent-solvent and solute–solvent pair potential for two particles a distance r apart is given by a Lennard-Jones potential,

$$u_{LJ}(r) = 4\epsilon\left[\left(\frac{\sigma}{r}\right)^{12} - \left(\frac{\sigma}{r}\right)^{6}\right]\Theta(R_c - r), \quad \text{(A.1)}$$

with parameters ϵ and σ and where $\Theta(x)=1$ for $x>0$ and is zero otherwise. Note that we have chosen the potential parameters the same for the solute and the solvent. For differing parameters the Lorentz-Berthelot, i.e. $\sigma_{12}=(\sigma_1+\sigma_2)/2$ and $\epsilon_{12}=\sqrt{\epsilon_1\epsilon_2}$, mixing rules could be applied. A simple procedure to correct the truncation of the Lennard-Jones potential is to add to the potential energy a self-term per particle [45],

$$u_{LJ}^{s} = \frac{8\pi}{3}\epsilon\sigma^3\left[\frac{1}{3}\left(\frac{\sigma}{R_c}\right)^9 - \left(\frac{\sigma}{R_c}\right)^3\right]. \quad \text{(A.2)}$$

In simulations done at constant volume and number of particles, this self-term (and the corresponding term for the polar interactions below) is a constant and could be added as a correction to the results after the simulation. However, in simulations in which volume or number of particles are varied for a particular simulation cell (like during simulations of the Gibbs ensemble), such a self-term changes under the corresponding ''moves''.

The dipolar part of the solvent-solvent pair potential for two particles at $\boldsymbol{r}_i$ and $\boldsymbol{r}_j$ with dipoles $\boldsymbol{\mu}_i$ and $\boldsymbol{\mu}_j$, including linearly tapered reaction field boundary conditions [46], is given by

$$u_{\mathrm{DD}}^{\mathrm{rf}}(\boldsymbol{r}_{ij},\boldsymbol{\mu}_i,\boldsymbol{\mu}_j)=\left[\left(\frac{1}{r_{ij}^3}-\frac{2(\epsilon'-1)}{(2\epsilon'+1)R_{\mathrm{eff}}^3}\right)\boldsymbol{\mu}_i\cdot\boldsymbol{\mu}_j-\frac{3(\boldsymbol{r}_{ij}\cdot\boldsymbol{\mu}_i)(\boldsymbol{r}_{ij}\cdot\boldsymbol{\mu}_j)}{r_{ij}^5}\right]t(r_{ij}) \tag{A.3}$$

with the tapering function

$$t(r)=\begin{cases}1, & r<R_{\mathrm{s}},\\ 1-(r-R_{\mathrm{s}})/(R_{\mathrm{c}}-R_{\mathrm{s}}), & R_{\mathrm{s}}<r<R_{\mathrm{c}},\\ 0, & R_{\mathrm{c}}<r,\end{cases} \tag{A.4}$$

with $\boldsymbol{r}_{ij}=\boldsymbol{r}_i-\boldsymbol{r}_j$, $r_{ij}=|\boldsymbol{r}_{ij}|$, the reaction field dielectric constant ϵ', and the switching radius $R_{\mathrm{s}}=fR_{\mathrm{c}}$ (we took $f=0.95$). R_{eff} is given by $R_{\mathrm{eff}}^3=(1+f+f^2+f^3)R_{\mathrm{c}}^3/4$. To correct for the truncation, a self-term per particle given by

$$u_{\mathrm{DD}}^{\mathrm{s}}=-\frac{\mu^2}{R_{\mathrm{eff}}^3}\frac{\epsilon'-1}{2\epsilon'+1} \tag{A.5}$$

is added to the electrostatic interaction energy.

The polar part of the solute–solvent pair potential is defined in accordance with the tapered reaction field boundary conditions to be

$$u_{\mathrm{QD}}^{\mathrm{rf}}(\boldsymbol{r}_{si},\boldsymbol{\mu}_i)=q\left(\frac{1}{r_{si}^3}-\frac{2(\epsilon'-1)}{(2\epsilon'+1)R_{\mathrm{eff}}^3}\right)\times(\boldsymbol{r}_{si}\cdot\boldsymbol{\mu}_i)t(r_{si}), \tag{A.6}$$

where the solute charge q is located at $\boldsymbol{r}_{\mathrm{s}}$. The self-energy term (a Born-energy in a sphere of radius R_{eff}) is given by

$$u_{\mathrm{QD}}^{\mathrm{s}}=-\frac{q^2}{R_{\mathrm{eff}}}\left(1-\frac{1}{\epsilon'}\right). \tag{A.7}$$

References

[1] M. Maroncelli, J. Mol. Liq. 57 (1993) 1.
[2] Y. Gauduel, P.J. Rossky (Eds.), Ultrafast reaction dynamics and solvent effects, AIP Conference Proceedings, vol. 298, AIP, New York, 1994.
[3] Structure fluctuation, and relaxation in solutions, Thematic issue of J. Mol. Liq., vol. 65-66, 1995.
[4] R.M. Stratt, M. Maroncelli, J. Phys. Chem. 100 (1996) 12981.
[5] M. Maroncelli, G.R. Fleming, J. Chem. Phys. 89 (1988) 5044.
[6] J.S. Bader, D. Chandler, Chem. Phys. Lett. 157 (1989) 501.
[7] M. Maroncelli, J. Chem. Phys. 94 (1991) 2084.
[8] E.A. Carter, J.T. Hynes, J. Chem. Phys. 94 (1991) 5961.
[9] E. Neria, A. Nitzan, J. Chem. Phys. 96 (1992) 5433.
[10] L. Perera, M.L. Berkowitz, J. Chem. Phys. 96 (1992) 3092.
[11] L. Perera, M.L. Berkowitz, J. Chem. Phys. 97 (1992) 5253.
[12] T. Fonseca, B.M. Ladanyi, J. Phys. Chem. 95 (1991) 2116.
[13] D.K. Phelps, M.J. Weaver, B.M. Ladanyi, Chem. Phys. 176 (1993) 575.
[14] T. Fonseca, B.M. Ladanyi, J. Mol. Liq. 60 (1994) 1.
[15] P.V. Kumar, M. Maroncelli, J. Chem. Phys. 103 (1995) 3038.
[16] T. Kalbfleisch, R. Fan, J. Roebber, P. Moore, E. Jacobsen, L.D. Ziegler, J. Chem. Phys. 103 (1995) 7673.
[17] T.S. Kalbfleisch, L.D. Ziegler, T. Keyes, J. Chem. Phys. 105 (1996) 7034.
[18] M.D. Stephens, J.G. Saven, J.L. Skinner, J. Chem. Phys. 106 (1997) 2129.
[19] S.A. Egorov, M.D. Stephens, J.L. Skinner, to appear in J. Chem. Phys.
[20] R.W. Shaw, T.B. Brill, A.A. Clifford, C.A. Eckert, E.U. Franck, Chem. Eng. News 69 (1991) 26.
[21] T.L. Chester, J.D. Pinkston, D.E. Raynie, Anal. Chem. 68 (1996) 487R.
[22] Y.-P. Sun, G. Bennett, K.P. Johnston, M.A. Fox, J. Phys. Chem. 96 (1992) 10001.
[23] Y.-P. Sun, C.E. Bunker, N.B. Hamilton, Chem. Phys. Lett. 210 (1993) 111.
[24] Y.-P. Sun, C.E. Bunker, Ber. Bunsenges. Phys. Chem. 99 (1995) 976.
[25] J.L. Fulton, D.M. Pfund, S.L. Wallen, M. Newville, E.A. Stern, Y. Ma, J. Chem. Phys. 105 (1996) 2161.
[26] H. Tanaka, J.W. Shen, K. Nakanishi, X.C. Zeng, Chem. Phys. Lett. 239 (1995) 168.
[27] M.E. van Leeuwen, Fluid Phase Equilibria 99 (1994) 1.

[28] C.D. Hall, K.A. Johnson, A.N. Burgess, N. Winterton, W.S. Howells, Molec. Phys. 74 (1991) 27.
[29] H. Gordon, S. Goldman, Mol. Simul. 2 (1989) 177.
[30] B. Garzón, S. Lago, C. Vega, Chem. Phys. Lett. 231 (1994) 366.
[31] A.Z. Panagiotopoulos, Molec. Phys. 61 (1987) 813.
[32] B. Smit, C.P. Williams, E.M. Hendriks, S.W. de Leeuw, Molec. Phys. 68 (1989) 765.
[33] M.E. van Leeuwen, B. Smit, E.M. Hendriks, Molec. Phys. 78 (1993) 271.
[34] M.E. van Leeuwen, Molec. Phys. 82 (1994) 383.
[35] K.K. Mon, K. Binder, J. Chem. Phys. 96 (1992) 6989.
[36] H.C. Andersen, J. Comput. Phys. 52 (1983) 24.
[37] H.C. Andersen, J. Chem. Phys. 72 (1980) 2384.
[38] B. Jayaram, R. Fine, K. Sharp, B. Honig, J. Phys. Chem. 93 (1989) 4320.
[39] D.Y.C. Chan, D.J. Mitchell, B.W. Ninham, J. Chem. Phys. 70 (1979) 2946.
[40] I. Rips, J. Klafter, J. Jortner, J. Chem. Phys. 88 (1988) 3246.
[41] I. Rips, J. Klafter, J. Jortner, J. Chem. Phys. 88 (1988) 4288.
[42] M. Maroncelli, V.P. Kumar, A. Papazyan, J. Phys. Chem. 97 (1993) 13.
[43] R. Olender, A. Nitzan, J. Chem. Phys. 102 (1995) 7180.
[44] P. Knödler, A. Nitzan, unpublished results.
[45] M.P. Allen, D.J. Tildesley, Computer simulation of liquids, Clarendon Press, Oxford, 1987.
[46] D.J. Adams, E.H. Adams, G.J. Hills, Mol. Phys. 38 (1979) 931.